Wavefield-continuation angle-domain common-image gathers for migration velocity analysis

Biondo Biondi*, Thomas Tisserant, Stanford University, William Symes, Rice University

SUMMARY

We analyze the kinematic properties of offset-domain Common Image Gathers (CIGs) and Angle-Domain CIGs (ADCIGs) computed by wavefield-continuation migration. Our results are valid regardless of whether the CIGs were obtained by using the correct migration velocity. They thus can be used as a theoretical basis for developing Migration Velocity Analysis (MVA) methods that exploit the velocity information contained in ADCIGs.

We demonstrate that in an ADCIG cube the image point lies on the normal to the apparent reflector dip, passing through the point where the source ray intersects the receiver ray. Starting from this geometric result, we derive an analytical expression for the expected movements of the image points in ADCIGs as functions of the traveltime perturbation caused by velocity errors. By applying this analytical result and assuming stationary raypaths, we then derive two expressions for the Residual Moveout (RMO) function in ADCIGs. We verify our theoretical results and test the accuracy of the proposed RMO functions by analyzing the migration results of a synthetic data set with a wide range of reflector dips.

We propose a 3-D extension of our kinematic analysis to the restricted, but in practice useful, case when the source ray and the receiver ray are coplanar. This leads to a 3-D generalization of the relationships used to compute ADCIGs from migrated images. We demonstrate the application of the 3-D transformation to angle domain on the image cube obtained from common-azimuth migration of the SEG-EAGE salt data set.

INTRODUCTION

With wavefield-continuation migration methods being used routinely for imaging project in complex areas, the ability to perform Migration Velocity Analysis (MVA) starting from the results of wavefield-continuation migration is becoming essential to advanced seismic imaging. As for Kirchhoff imaging, MVA for wavefield-continuation imaging is mostly based on the information provided by the analysis of Common Image Gather (CIGs). Most of the current MVA methods start from Angle-Domain CIGs (ADCIGs) (Biondi and Sava, 1999; Clapp and Biondi, 2000; Mosher et al., 2001; Liu et al., 2001), though the use of more conventional surface-offset-domain CIGs is also being evaluated (Stork et al., 2002).

In this paper we analyze the use of ADCIGs for MVA in a "ray tomography" framework, in contrast with their use in a "wave-equation" framework by Biondi and Sava (1999) and Sava and Biondi (2003). MVA from ADCIGs computed using wavefield-continuation migration is conceptually analogous to MVA from conventional offset-domain CIGs obtained by Kirchhoff migration (Clapp and Biondi, 2000). The ADCIGs are analyzed for departure from flatness, usually by applying some kind of Residual Moveout (RMO) analysis. The RMO analysis provides measurements of depth errors that are first transformed into traveltime perturbations and finally inverted into velocity perturbations by a ray-based tomographic inversion. This process is repeated several times in order to converge to a satisfactory result.

For the information contained in the ADCIG to be properly inverted into velocity updates, we need to perform accurately the following two tasks: 1) measure velocity errors from ADCIGs by residual moveout (RMO) analysis, and 2) relate RMO measurements to perturbations in the kinematics of the events. Our kinematic analysis leads to the definition of accurate relationships that can be applied to improve these two tasks. Our analysis demonstrates that in an ADCIG cube the image point lies on the normal to the apparent reflector dip passing through the point where the source ray intersects the receiver ray. We exploit this result to define an analytical expression for the expected movements of the image points in AD-CIGs as a function of the traveltime perturbation caused by velocity errors. This leads us to the definition of two alternative residual moveout functions that can be applied when measuring velocity errors from migrated images.

Our analysis is valid for arbitrary reflector dip, and even for over-turned events. However, it is based on the assumption that the source and receiver rays are coplanar. This assumption is valid in 2-D, but it limits the generality of our results in 3-D. The last section of this abstract discusses the application of our results to 3-D.

KINEMATIC PROPERTIES OF ADCIGS

The computation of ADCIGs is based on a decomposition (usually performed by slant-stacks) of the wavefield either before imaging (Mosher et al., 1997; Prucha et al., 1999; Xie and Wu, 2002), or after imaging (Sava and Fomel, 2002; Rickett and Sava, 2002; Biondi and Shan, 2002). In either case, the slant stack transformation is usually applied along the horizontal subsurface-offset axis. However, when the geologic dips are steep, this "conventional" way of computing CIGs does not produce useful gathers, even if it is kinematically valid for geologic dips milder than 90 degrees. As the geologic dips increase, the horizontal-offset CIGs (HOCIGs) degenerate, and their focusing around zero offset blurs. This limitation of HOCIGs can be sidestepped by computing offset-domain CIGs along the vertical subsurface-offset axis (VOCIGs) (Biondi and Shan, 2002). Although neither set of offset-domain gathers (HOCIG or VOCIG) provides useful information for the whole range of geologic dips, an appropriate combination of the two sets does. Biondi and Symes (2003) present a simple and effective method for combining a HOCIG cube with a VOCIG cube to create an ADCIG cube that is immune to artifacts in the presence of arbitrary geologic dips.

Figure 1 illustrates the geometry of the different kinds of offset-domain CIGs for a single event. In this sketch, the migration velocity is assumed to be lower than the true velocity, and thus the reflections are imaged too shallow and above the point where the source ray crosses the receiver ray ($\bar{I}$). The line passing through $\bar{I}$, and bisecting the angle formed by the source and receiver ray, is oriented at an angle α with respect to the vertical direction. The angle α is the apparent geological dip of the event after imaging. Half of the angle formed between the source and receiver ray is the apparent aperture angle γ.

Figure 2 illustrates how the events imaged in the offset domain (Figure 1) move when the image is transformed into the angle domain. It can be demonstrated that, independently from the migration method employed to compute them, all ADCIGs enjoy the the following important property:

- The image location in the angle domain (I_γ) lies on the normal to the apparent geological dip passing through the crossing point of the source and receiver rays ($\bar{I}$). I_γ is located at the crossing point of the lines passing through S_0 and R_0 and orthogonal to the source ray and receiver ray, respectively. The total normal shift caused by incomplete focusing at zero offset is equal to:

$$\Delta \mathbf{n}_{\text{tot}} = \left(I_\gamma - \bar{I} \right) = \Delta \mathbf{n}_{h_0} \left(1 + \tan^2 \gamma \right) = \frac{\Delta \mathbf{n}_{h_0}}{\cos^2 \gamma}, \quad (1)$$
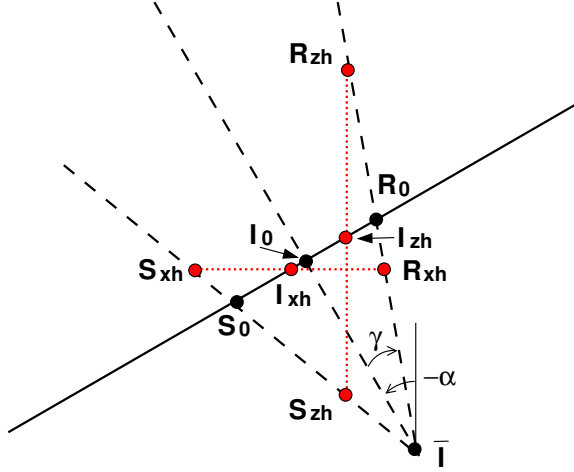
Wavefield-continuation ADCIGs for MVA

Figure 1: Geometry of the three different kinds of offset-domain (horizontal, vertical and geological-dip) CIG for a single event migrated with the wrong velocity. I_{x_h} is the horizontal-offset image point, I_{z_h} is the vertical-offset image point, and I_0 is the geological-dip offset image point.
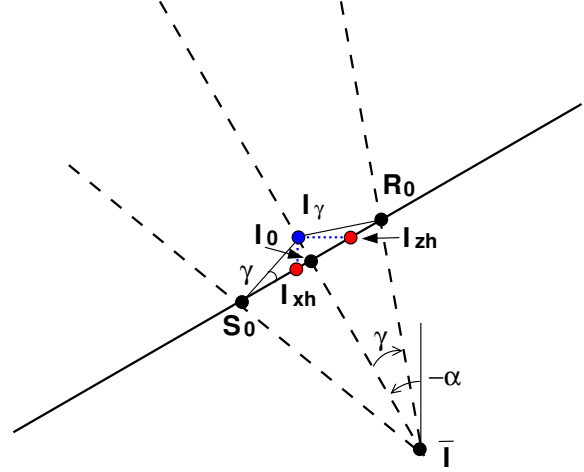

Figure 2: Geometry of an angle-domain CIG for a single event migrated with the wrong velocity. The transformation to the angle domain shifts all the offset-domain image points (I_{x_h}, I_{z_h}, I_0) to the same angle-domain image point I_γ. The shift from $\bar{I}$ to I_γ that is induced by the velocity error is defined in equation (1).

where $\Delta\mathbf{n}_{h_0} = (I_0 - \bar{I})$ is the normal shift in the geological-dip offset domain.

From equation (1), invoking Fermat's principle, we can also easily derive a relationship between the total normal shift $\Delta\mathbf{n}_{\text{tot}}$ and the total traveltime perturbation caused by velocity errors as follows:

$$\Delta\mathbf{n}_{\text{tot}} = -\frac{\Delta t}{2S\cos\gamma}\mathbf{n}, \tag{2}$$

where S is the background slowness around the image point and Δt is defined as the difference between the perturbed traveltime and the background traveltime.

The analytical relationship between reflector movement and traveltime perturbation expressed in equation (2) is verified by the numerical experiment shown in Figure 3. This figure compares the images of a spherical reflector obtained using a low migration velocity (slowness scaled by $\rho = 1.04$) with the reflector position computed analytically under the assumption that I_γ is indeed the image point in an ADCIG. Because both the true and the migration velocity functions are constant, the migrated reflector location can be computed exactly by a simple "kinematic migration" of the recorded events. This process takes into account the difference in propagation directions between the "true" events and the "migrated" events caused by the scaling of the velocity function. The images shown in the six panels in Figure 3 correspond to six different apparent aperture angles: a) $\gamma_\rho = 0$, b) $\gamma_\rho = 10$, c) $\gamma_\rho = 20$, d) $\gamma_\rho = 30$, e) $\gamma_\rho = 40$, f) $\gamma_\rho = 50$. The black lines superimposed onto the images are the corresponding reflector locations predicted by the analytical "kinematic migration". The analytical lines perfectly track the analytical images for all values of γ_ρ.

RESIDUAL MOVEOUT IN ADCIGS

The inconsistencies between the migrated images at different aperture angles are the primary source of information for velocity updating during Migration Velocity Analysis (MVA). An effective and robust method for measuring inconsistencies between images is to compute semblance scans as a function of one "residual moveout" (RMO) parameter, and then pick the maxima of the semblance

scan. This procedure is most effective when the residual moveout function used for computing the semblance scans closely approximates the true moveouts in the images.

Applying the kinematic properties discussed in the previous section, Biondi and Symes (2003) derived two expressions for the RMO shift along the normal to the reflector ($\Delta\mathbf{n}_{\text{RMO}}$), under the assumptions of stationary raypaths and constant scaling of the slowness function by a factor ρ. The first expression is:

$$\Delta\mathbf{n}_{\text{RMO}} = \frac{1-\rho}{1-\rho(1-\cos\alpha)}\frac{\sin^2\gamma}{(\cos^2\alpha - \sin^2\gamma)}z_0\,\mathbf{n}, \tag{3}$$

where z_0 is the depth at normal incidence. The second RMO function is directly derived from the first by assuming flat reflectors ($\alpha = 0$):

$$\Delta\mathbf{n}_{\text{RMO}} = (1-\rho)\tan^2\gamma z_0\,\mathbf{n}. \tag{4}$$

As expected, in both expressions the RMO shift is null at normal incidence ($\gamma = 0$), and when the migration slowness is equal to the true slowness ($\rho = 1$).

Figure 4 illustrates the accuracy of the two RMO functions when predicting the actual RMO in the migrated images obtained with a constant slowness function with $\rho = 1.04$. The four panels show the ADCIGs corresponding to different apparent reflector dip: a) $\alpha = 0$; b) $\alpha = 30$; c) $\alpha = 45$; d) $\alpha = 60$. Notice that the vertical axes change across the panels; in each panel the vertical axis is oriented along the direction normal to the respective apparent geological dip. The solid lines superimposed onto the images are computed using equation (3), whereas the dashed lines are computed using equation (4). The solid lines overlap the migration results for all dip angles. This figure demonstrates that, when the slowness perturbation is sufficiently small (4 % in this case), the assumption of stationary raypaths causes only small errors in the predicted RMO.

EXTENSION TO 3-D

The analysis of the kinematic properties of ADCIGs presented in the previous sections is based on the assumption that the source and receiver rays cross, even when the data were migrated with
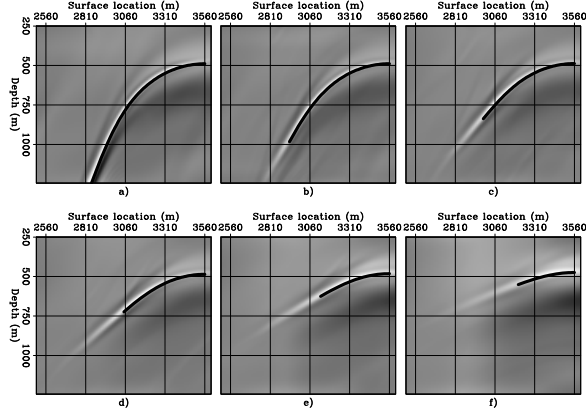
Figure 3: Comparison of the actual images obtained using a low migration velocity, with the reflector position computed analytically under the assumption that the image point lies on the normal to the apparent geological dip (I_γ in Figure 2). The black lines superimposed onto the images are the reflector locations predicted analytically. The six panels correspond to six different apparent aperture angles: a) $\gamma_\rho = 0$ b) $\gamma_\rho = 10$ c) $\gamma_\rho = 20$ d) $\gamma_\rho = 30$ e) $\gamma_\rho = 40$ f) $\gamma_\rho = 50$.
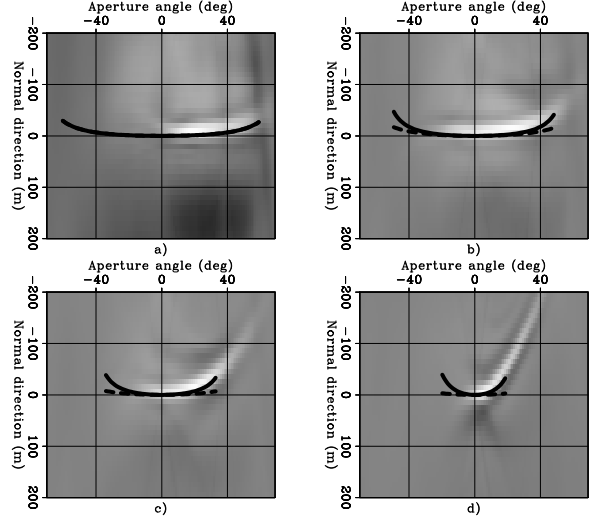

Figure 4: ADCIGs for four different apparent reflector dips: a) $\alpha = 0$; b) $\alpha = 30$; c) $\alpha = 45$; d) $\alpha = 60$ with $\rho = 1.04$. Superimposed onto the images are the RMO functions computed using equation (3) (solid lines), and using equation (4) (dashed lines). Notice that the vertical axes change across the panels; in each panel the vertical axis is oriented along the direction normal to the respective apparent geological dip.

the wrong velocity. This assumption is valid in 2-D except in degenerate cases of marginal practical interest (e.g. diverging rays). In 3-D, this assumption is more easily violated, because the two rays are not always coplanar. This discrepancy between 2-D and 3-D geometries makes the full generalization to 3-D of our results less than trivial. However, if we restrict our analysis to the practically important cases when the assumption of coplanarity between the source and receiver ray is fulfilled (at least approximately) we can then extend the 2-D analysis to 3-D. In particular the analytical relationships presented in equation (1) and equation (2) are still valid. However, in 3-D the transformation of offset-domain gather into angle gather needs to take into account the angle between the source-receiver azimuth and the azimuth of the normal to the reflector. Consequently, the relationships presented in (Sava and Fomel, 2002; Rickett and Sava, 2002; Biondi and Shan, 2002) need to be revised.

Common-azimuth migration

The simplest 3-D extension is to the case when common-azimuth downward-continuation is used to migrate the data (Biondi and Palacharla, 1996). In this case, the cross-line dip δ enters in the relationship between the aperture angle γ and the in-line offset wavenumber $k_{h\,x}$ and the vertical wavenumber k_z as a simple cosine scaling factor; that is:

$$\tan\gamma = \frac{k_{h\,x}}{k_z}\cos\delta. \qquad (5)$$

Equation (5) is easily expressed in the wavenumber domain as:

$$\tan\gamma = \frac{k_{h\,x}}{\sqrt{k_z^2 + k_{m\,y}^2}}, \qquad (6)$$

where $k_{m\,y}$ is the cross-line midpoint wavenumber.

We applied the 3-D transformation to angle domain on the image cube obtained from common-azimuth migration of the SEG-EAGE salt dataset. Figure 5 shows a depth slice taken at a depth of 580 meters. Figure 6 shows two ADCIGs taken at in-line location of

8,350 meters and cross-line location of 5,250 meters. This location corresponds to the crossing point of the grid lines in Figure 5. The ADCIG on the left was computed using the 2-D relationship for the transformation to angle domain [i.e. equation (6) with $k_{m\,y}$ set to zero]. The ADCIG on the right was computed using the correct 3-D relationship [i.e. equation (6)]. The $\cos\delta$ term corrects the ADCIG for the top of the salt reflection ($z \approx 580$ meters) that dips at approximately 50 degrees in the cross-line direction. Notice that the bottom of the salt reflection ($z \approx 2,100$ meters) is unaffected by the $\cos\delta$ term because it is flat.

Full prestack migration

The general case is more complex than the common-azimuth case, but it can be reduced to the common-azimuth case by applying the *coplanarity condition* presented by Biondi (2003), and expressed as:

$$k_{h\,y} = \frac{k_{m\,y}k_{m\,x}k_{h\,x}}{k_z\sqrt{k_z^2 + k_{m\,y}^2}}; \qquad (7)$$

where $k_{m\,x}$ is the in-line midpoint wavenumber, and $k_{h\,y}$ is the cross-line offset wavenumber. Equation (7) defines a path in the offset wavenumber plane along which relationship (6) should be evaluated.

CONCLUSIONS

We presented a kinematic analysis of the ADCIGs obtained from wavefield-continuation migration when the events are not perfectly focused because of errors in migration velocity. The kinematic analysis leads to the derivation of the fundamental relationships to: 1) measure residual moveout from ADCIGs, and 2) relate measured reflector movements to perturbations in the kinematics of the events. The results of our analysis are valid for arbitrary reflector dip and thus they can be directly applied to improve the MVA process in presence of complex geological structure. We also presented a 3-D extension of the offset-to-angle transformation of
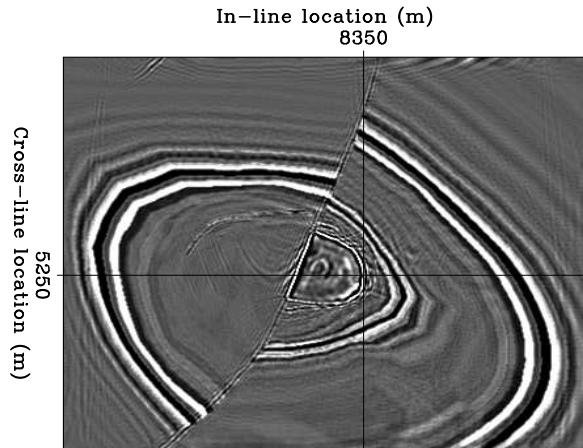
Wavefield-continuation ADCIGs for MVA

Figure 5: Depth slice cut through the common-azimuth image of the SEG-EAGE salt dataset at a depth of 580 meters. The crossing point of the grid lines indicates the location of the ADCIGs shown in Figure 6.
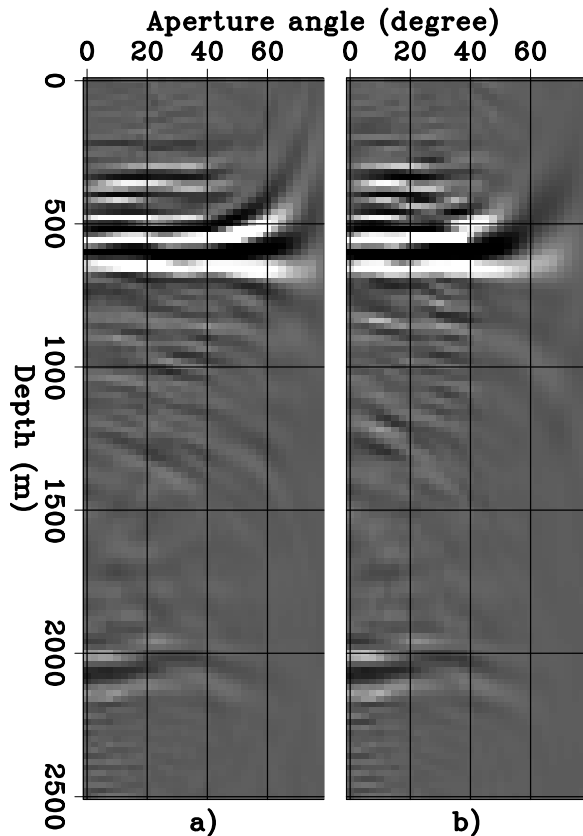

Figure 6: ADCIGs taken at in-line location of 8,350 meters and cross-line location of 5,250 meters: a) computed using the 2-D relationship for the transformation to angle domain [i.e. equation (6) with k_{m_y} set to zero]. b) computed using the correct 3-D relationship [i.e. equation (6)].

CIGs, and demonstrate its application to the image cube obtained from common-azimuth migration of the SEG-EAGE salt data set.

ACKNOWLEDGMENTS

REFERENCES

Biondi, B., and Palacharla, G., 1996, 3-D prestack migration of common-azimuth data: Geophysics, **61**, no. 6, 1822–1832.

Biondi, B., and Sava, P., 1999, Wave-equation migration velocity analysis:, *in* 69th Ann. Internat. Mtg Soc. of Expl. Geophys., 1723–1726.

Biondi, B., and Shan, G., 2002, Prestack imaging of overturned reflections by reverse time migration:, *in* 72nd Ann. Internat. Mtg Soc. of Expl. Geophys., 1284–1287.

Biondi, B., and Symes, W., 2003, Angle-domain common-image gathers for migration velocity analysis by wavefield-continuation imaging: Geophysics, submitted for publication.

Biondi, B., 2003, Narrow-azimuth migration of marine streamer data:, *in* 73rd Ann. Internat. Mtg Soc. of Expl. Geophys., submitted.

Clapp, R., and Biondi, B., 2000, Tau domain migration velocity analysis using angle CRP gathers and geologic constrains:, *in* 70th Ann. Internat. Mtg Soc. of Expl. Geophys., 926–929.

Liu, W., Popovici, A., Bevc, D., and Biondi, B., 2001, 3-D migration velocity analysis for common image gathers in the reflection angle domain:, *in* 71st Ann. Internat. Mtg Soc. of Expl. Geophys., 885–888.

Mosher, C. C., Foster, D. J., and Hassanzadeh, S., 1997, Common angle imaging with offset plane waves:, *in* 67th Ann. Internat. Mtg Soc. of Expl. Geophys., 1379–1382.

Mosher, C., Jin, S., and Foster, D., 2001, Migration velocity analysis using common angle image gathers:, *in* 71st Ann. Internat. Mtg Soc. of Expl. Geophys., 889–892.

Prucha, M., Biondi, B., and Symes, W., 1999, Angle-domain common-image gathers by wave-equation migration: 69th Ann. Internat. Meeting, Soc. Expl. Geophys., Expanded Abstracts, 824–827.

Rickett, J., and Sava, P., 2002, Offset and angle-domain common image-point gathers for shot-profile migration: Geophysics, **67**, 883–889.

Sava, P., and Biondi, B., 2003, Wave-equation migration velocity analysis by inversion of differential image perturbations:, *in* 73rd Ann. Internat. Mtg Soc. of Expl. Geophys., submitted.

Sava, P., and Fomel, S., 2002, Angle-domain common-image gathers by wavefield continuation methods: Geophysics, accepted for publication.

Stork, C., Kitchenside, P., Yingst, D., Albertin, U., Kostov, C., Wilson, B., Watts, D., Kapoor, J., and Brown, G., 2002, Comparison between angle and offset gathers from wave equation migration and Kirchhoff migration:, *in* 72nd Ann. Internat. Mtg Soc. of Expl. Geophys., 1200–1203.

Xie, X. B., and Wu, R. S., 2002, Extracting angle domain information from migrated wavefield:, *in* 72nd Ann. Internat. Mtg Soc. of Expl. Geophys., 1360–1363.